

MDPI

Review

Ultrafast Pulse Generation from Quantum Cascade Lasers

Feihu Wang 1,2,3,*0, Xiaoqiong Qi 40, Zhichao Chen 1,2,30, Manijeh Razeghi 5 and Sukhdeep Dhillon 6

- Shenzhen Institute for Quantum Science and Engineering, Southern University of Science and Technology, Shenzhen 518055, China
- International Quantum Academy, Shenzhen 518048, China
- ³ Guangdong Provincial Key Laboratory of Quantum Science and Engineering, Southern University of Science and Technology, Shenzhen 518055, China
- School of Information Technology and Electrical Engineering, The University of Queensland, Brisbane, OLD 4072, Australia
- Center for Quantum Devices, Department of Electrical Engineering and Computer Science, Northwestern University, Evanston, IL 60208, USA
- 6 Laboratoire de Physique de l'Ecole Normale Supérieure, ENS, Université PSL, CNRS, Sorbonne Université, Université de Paris, 75014 Paris, France
- * Correspondence: wangfh@sustech.edu.cn

Abstract: Quantum cascade lasers (QCLs) have broken the spectral barriers of semiconductor lasers and enabled a range of applications in the mid-infrared (MIR) and terahertz (THz) regimes. However, until recently, generating ultrashort and intense pulses from QCLs has been difficult. This would be useful to study ultrafast processes in MIR and THz using the targeted wavelength-by-design properties of QCLs. Since the first demonstration in 2009, mode-locking of QCLs has undergone considerable development in the past decade, which includes revealing the underlying mechanism of pulse formation, the development of an ultrafast THz detection technique, and the invention of novel pulse compression technology, etc. Here, we review the history and recent progress of ultrafast pulse generation from QCLs in both the THz and MIR regimes.

Keywords: quantum cascade lasers; mode-locking; ultrafast dynamics; terahertz and mid-infrared; semiconductor lasers; pulse compression; laser physics

org/10.3390/ 1. Introduction

Quantum cascade lasers (QCLs) are electrically pumped compact semiconductor light sources that were first demonstrated in the mid-infrared in 1994 by Faist et al. at Bell Lab [1] and in the terahertz (THz) frequency range by Köhler et al. at Scuola Normale Superiore in 2002 [2]. The OCL concept has enabled powerful and compact coherent light sources in previously inaccessible or unpractical mid-infrared and THz regions of the electromagnetic spectrum. In the mid-infrared area, QCLs have achieved an impressive performance with more than 5.6 W output power from a single facet [3-6], and with high wall-plug efficiency up to 31% at room temperature (RT) in a continuous wave (CW) operation [7]. Besides, high beam-quality single-mode long-wave infrared (LWIR) QCLs with record light extraction (2.0 MW cm⁻² sr⁻¹ for $\lambda \approx 10 \ \mu m$, 2.2 MW cm⁻² sr⁻¹ for $\lambda \approx 9 \ \mu m$, 5.0 MW cm⁻² sr⁻¹ for $\lambda \approx 8 \ \mu m$) from a single facet in CW operation at 15 °C have also been demonstrated [8]. These results mark an important milestone in the lighting capability of inter-sub-band semiconductor lasers in the mid-infrared spectral ranges. Beyond the Restrahlen band (>50 μm), QCLs have also shown remarkable development: high output power over 1 W, far-field engineering on metal-metal waveguide, quantum limited linewidths and self-generated frequency combs have been demonstrated [9–13]. Although there remain challenges, the further development and exploitation of QCLs is crucial due to the unparalleled success of these devices in terms of their output power and wavelength agility in a compact, potentially inexpensive and user-friendly geometry.



Citation: Wang, F.; Qi, X.; Chen, Z.; Razeghi, M.; Dhillon, S. Ultrafast Pulse Generation from Quantum Cascade Lasers. *Micromachines* **2022**, *13*, 2063. https://doi.org/10.3390/ mi13122063

Academic Editor: Francesco Ruffino

Received: 16 October 2022 Accepted: 8 November 2022 Published: 24 November 2022

Publisher's Note: MDPI stays neutral with regard to jurisdictional claims in published maps and institutional affiliations



Copyright: © 2022 by the authors. Licensee MDPI, Basel, Switzerland. This article is an open access article distributed under the terms and conditions of the Creative Commons Attribution (CC BY) license (https://creativecommons.org/licenses/by/4.0/).

Micromachines 2022, 13, 2063 2 of 18

Mode-locking of QCLs enables the gathering of mid-infrared and THz energy on a very short timescale and generation of periodic light pulses in a long-term time domain. It offers unique conditions and an extreme environment for the development of cutting-edge technology, the test of fundamental physics, the examination of relativity theory, and expansion of the boundaries of human cognition, etc. [14–18]. Unlike traditional semi-conductor lasers, mode-locking of QCLs has proven to be extremely challenging due to its ultrafast gain recovery time, which is more than one order of magnitude smaller than the round-trip time of photons that are circling in the laser cavity [19–21]. However, this stumbling block was overcome in 2011 by injecting a round-trip electrical modulation to force pulse formation within the laser cavity [22]. Thereafter, ultrafast QCLs have undergone considerable development, including the explanation of the underlying physics of mode-locking [23–25], pulse shortening by a novel dispersion compensation technique [26], and other pulse-generation and compression techniques [24,27,28].

Here, we focus on discussing the development of ultrafast pulse generation from QCL, and divide the main content of this review paper into four sections, as follows: (I) in the first section, we give an introduction to the ultrafast dynamics of QCLs from the theoretical aspect [28–31]; (II) in the second section, we present the high-speed modulation of QCLs using a radio-frequency (RF) injection locking; (III) in the third section we present the mode-locked QCLs [22,32–35]; (IV) in the fourth section, we present the state-of-art results of ultrafast pulse generation from THz QCLs [26], and (V) in the fifth section we present pulse generation in MIR-QCLs by applying novel compression techniques [24,27].

2. Ultrafast Dynamics of QCLs

As unipolar devices, photon emission in QCLs is based on intersubband transitions in the conduction band of quantum heterostructures. They exhibit ultra-short carrier lifetimes that are on the same (picosecond) scale as the photon lifetime, which leads to the absence of the relaxation resonant oscillations in the transient response of these devices and ultrafast gain dynamics. The ultrafast gain dynamics of QCLs, combined with Kerr nonlinearities, the group velocity dispersions (material dispersion, waveguide dispersion, and gain dispersion), and spatial hole burning determine the pulse formation dynamics in QCLs. These intersubband transitions feature strong third-order optical nonlinearities, due to the large optical matrix element between the excited states and the empty lower states, allowing parametric processes due to four-wave mixing (FWM) [36]. Through the cascade FWM process based on multiple laser longitudinal modes and low group velocity dispersion (GVD), free-running combs with frequency modulations have been achieved in MIR-QCLs (this is frequency modulated QCLs and hence in principle no pulse generation) [36,37]. In addition, it has been found that a finite linewidth enhancement factor in fast gain medium lasers leads to a considerable Kerr nonlinearities, more so than in interband lasers with slow gain dynamics, which means that shorter carrier lifetimes lead to a wider FWM gain bandwidth, which in turn supports wider multi-mode emission [37]. Carrier lifetimes in THz QCLs are an order of magnitude higher than that in MIR-QCLs, which in principle make pulse formation in THz QCLs easier than in MIR-QCLs. However, the semiconductor material is more dispersive at THz frequencies than in mid-infrared frequencies due to stronger coupling with the crystalline lattice (for instance, GVD of GaAs at 40 K at 3.5 THz is 250 times higher that at 7 µm) [12], thus dispersion compensation techniques, such as a chirped corrugation etched into the facet of the laser [12] or GTIs [26], have to be considered to form stable pulses. In multi-mode QCLs with Fabry-Perot cavities, the waves travelling in forward and backward directions are coupled as they share the same gain medium, which gives rise to spatial hole burning (SHB) that favors multi-mode emission and can help to further reduce the pulse duration of the short pulses in QCLs. However, on the other hand, SHB also results in pulse instabilities and non-stationary pulse generation [38]. Furthermore, it has been concluded that the combined effects of SHB, GVD and Kerr nonlinearities due to asymmetric gain give rise to the recently observed linear frequency chirp [39]. The self-starting frequency combs generated in QCLs can be

Micromachines 2022, 13, 2063 3 of 18

improved by RF injection through active mode-locking [22,23] and even with harmonic mode-locking [28], which provides possibilities for higher repetition rates beyond the limitation from the laser cavity length. Recently, soliton structures have been observed in ring QCLs, which opens interesting physics questions in the lasers with fast gain dynamics.

The theoretical models used to investigate multi-mode dynamics and QCL combs include reduced rate equations [40,41], Maxwell Bloch equations [25,42], and Master equations [29,39,43,44]. The multi-mode reduced rate equations (Equations (1)–(4)) are based on interactions between electrons and photons through stimulated emissions, spontaneous emission, and stimulated absorptions. This model is very suitable for studying the time-resolved electron and photon transport dynamics and the steady-state analysis of the laser, such as light-current-voltage (LIV) curves. This model has been used to study the frequency tuning mechanisms [40] and ultra-fast mode switching dynamics in coupled-cavity QCLs [29]. It is also adapted to include the external perturbations into the model, such as optical injections and optical feedback effects. The model has been used to study single-mode and multi-mode dynamics under optical feedback in QCLs [41]. However, as rate equations, this model does not include spatial dependence effects, such as SHB.

$$\frac{dN_3(t)}{dt} = \frac{\eta_3 I}{q} - \sum_m G_m(N_3(t) - N_2(t)) S_m(t) - \frac{N_3(t)}{\tau_3},\tag{1}$$

$$\frac{dN_2(t)}{dt} = \frac{\eta_2 I}{q} + \sum_m G_m(N_3(t) - N_2(t))S_m(t) + \frac{N_3(t)}{\tau_{32}} + \frac{N_3(t)}{\tau_{sp}} - \frac{N_2(t)}{\tau_2},\tag{2}$$

$$\frac{dS_m(t)}{dt} = MG_m(N_3(t) - N_2(t))S_m(t) + \frac{M\beta_{\rm sp}N_3(t)}{\tau_{\rm sp}} - \frac{S_m(t)}{\tau_{\rm p,m}},\tag{3}$$

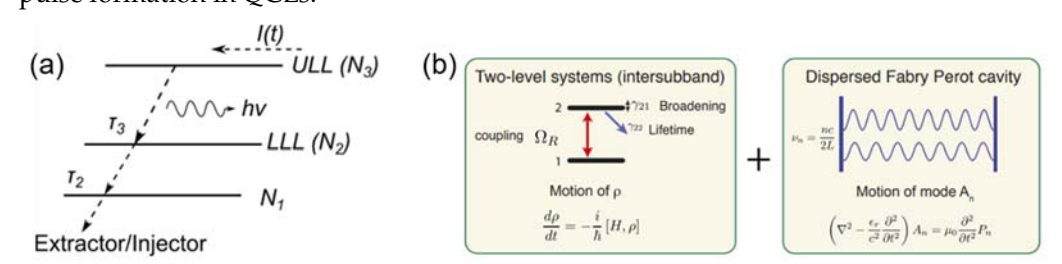
$$\frac{d\varphi_m(t)}{dt} = \frac{\alpha}{2} \left(MG_m(N_3(t) - N_2(t)) - \frac{1}{\tau_{p,m}} \right),\tag{4}$$

where $N_3(t)$ and $N_2(t)$ are the carrier populations in the upper and lower laser levels of the active medium (ULL and LLL), respectively, and $S_m(t)$ and $\varphi_m(t)$ are the photon population and the phase of the electric field in longitudinal mode m. The other input parameters include the injection efficiencies into ULL and LLL η_3 and η_2 , the drive current I, the number of periods in the active cavity M, spontaneous emission factor $\beta_{\rm sp}$, the carrier lifetimes τ_3 , τ_{32} , τ_2 and photon lifetime τ_p , the spontaneous emission lifetime $\tau_{\rm sp}$, the linewidth enhancement factor α and the gain factor for mode m G_m . The gain recovery time in QCLs can be described by the total carrier lifetime in ULL τ_3 in this model. The dependence of the optical gain on the population inversion and the amplitude-to-phase coupling are also included in this model.

The Maxwell–Bloch equations combine the Bloch equation and the wave equation, and are a set of equations for the normalized envelope of the electric field, the polarization, and the population inversion in the gain medium. By considering the polarization of the electric field, which describes the interactions between the laser field and the gain medium, this model includes the effects of Kerr nonlinearities through the optical susceptibility. It also includes the coherent coupling between the populations, such as Risken–Nummedal–Graham–Haken (RNGH) instabilities induced by the coherent resonant tunneling between adjacent stages in the active region. In addition, this model has time and spatial (only z direction) as independent parameters, which can include the SHB effects originated from the standing waves in the FP laser cavities, which play an important role on multimode operation and pulse duration reduction in the QCL combs study. This model has been used to investigate self-starting mode-locking and the formation of optical instabilities in QCLs [45,46]. However, as a full model, it is difficult to understand the roles of each of the physical effects on the formed frequency combs or pulses in the QCLs.

The conventional Haus Master equation can be used to study how the pulse shape varies under the gain dispersion and Kerr nonlinearities in conventional diode lasers where the gain dynamics are not fast, such that the gain recovery time is longer than one instabilities in QCLs [45,46]. However, as a full model, it is difficult to understand the roles of each of the physical effects on the formed frequency combs or pulses in the QCLs.

The conventional Haus Master equation can be used to study how the pulse shape varies under the gain dispersion and Kerr nonlinearities in conventional diode lasers where the gain dynamics are not fast, such that the gain recovery time is longer than one laser round trip time as shown in Figure 1 [47]. Despite its popularity, the Haus Master laser tionaphrine time as shown in Figure 1 [47]. Despite its popularity, the Haus Master laser tionaphrine time as shown in Figure 1 [47]. Despite its popularity, the Haus Master laser tionaphrine time as shown in Figure 1 [47]. Despite its popularity, the Haus Master laser time the test of the figure 1 [47]. The conventional master time the state of the figure 1 [47]. The conventional master requires sufficiently allowed the conventional master requires sufficiently allowed the conventional master requires and pronounced coherent effects. First the conventional master requires for amplitude modulated coherent effects. Furthermore, the Haus Master equation does not include coherent effects. Furthermore, the Haus Master equation does not include coherent effects. Furthermore, the Haus Master equation does not include coherent effects. Furthermore, the Haus Master equation does not include coherent of the state of the phase dynamics. The coherent master equation is more suitable for the phase dynamic. However, the Haus Master equation has recently been developed into the coherent Master equation is more suitable for modeling OCLs. The reduced Master equation is more suitable for modeling OCLs. The reduced Master equation can be used to reproduce the behavior of frequency modulation combs in OCLs and study the roles of SHB, FWM and GVD on the pulse formation in OCLs.



Higher 1 Th That bearest colored else essectively industrial transfer and essentis read of regression is one sin (QChs: (h) the electroperation and the colored data wile properties and the colored data wile properties and the constant of the colored data will be the colored data and the constant of the colored data will be the colored data and the constant of the colored data and the colored data an

3. INFIlmication Loading of QCIIs

modes as given in Equation (5):

Injection locking was originally used to transfer the spectral purity and stability of a master laser to a slave laser [18,49]. Typically, the master laser is a low-power spectrally pure laser, but the slave laser is a high-power and spectrally broad laser. When an optical seed from the master laser is injected into the cavity of the slave one, the slave laser can inherit the spectral and noise properties of the master laser. Simultaneously, the slave laser sized site no intain high prover to undipsing in these being above seed and various easier them philipation and stabilization for sized angles laser after your every broadband of the target is a long to the parties of the master laser. The provered the parties of the master laser after your every broadband of the proventies of the parties of the partie

brid mode-focking of inter-band semi-conductor lasers [50–52]. Here, we emphasize this from theoretical and experimental aspects as it is the underpinning approach for ultrafast pulse generation and active mode-locking of QCLs. When injection locking is presented, the beatnote of a laser has to be mentioned. In a QCL system, the beatnote is a series of discrete RF signals arising from the electrical QCL system, the beatnote is a series of discrete RF signals arising from the electrical QCL system, the beatnote is a series of discrete RF signals arising from the electrical Deathbeating of any two Fabry-Perot modes (f₁₊₁ – f₁). For a 3-mm-long QCL cavity, the beatnote frequency is close to 13 GHz, as well as its harmonics at 26 GHz, 39 GHz. The frequency is close to 13 GHz, as well as its harmonics at 26 GHz, 39 GHz. The frequency is close to 13 GHz, as well as its harmonics at 26 GHz, 39 GHz. The frequency is close to 13 GHz, as well as its harmonics at 26 GHz, which can mental beatnote is the most important parameter for active mode-locking, which can be expressed as the sum of the frequency difference between any two adjacent longitudinal

$$S(f) = \sum S_i (f_{n+1} - f_n)$$
(5)

Micromachines 2022, 13, 2063 5 of 18

The full width at half maximum (FWHM) of the beatnote signal is dominated by the frequency jittering of QCL modes. Similar to optical injection locking, by injecting an RF signal (f_{RF}) that is resonant with the FSR or beatnote ($f_{beatnote}$) into the QCL system, the spectral purity and stability of the low-noise external RF signal can be transferred to the QCL. From the complex amplitude evolution of the RF field in the system, the injection locking can be described using the following equation [53]:

$$\frac{d\varphi}{dt} = \omega_{RF} - \Delta\omega - \omega_L \sin\varphi \tag{6}$$

The injection-locking theory developed by *Adler* to describe the behavior of coupled nonlinear electronic oscillators [53]. However, it is ubiquitous in physical systems involving frequency locking between several oscillators such as lasers, mechanical oscillators, gyroscopes, etc. In Equation (6), φ represents the phase difference between the RF signal and the QCL internal electrical beating signal, ω_{RF} is the angular frequency of the RF signal, $\Delta \omega$ is the angular frequency of the beatnote, and ω_{L} is the locking range, which can be further given in the following equation [54]:

$$\omega_L = \frac{2\omega_0}{Q} \sqrt{\frac{P_{inj}}{P_0}} \tag{7}$$

In Equation (7), ω_0 is the free-running oscillation angular frequency, Q is the oscillator q-factor, P_{inj} is the injected power of RF source and P_0 is the optical power within the laser cavity. When the condition $|\omega_{RF} - \Delta\omega| < \omega_L$ is satisfied, Equation (6) has a steady-state solution: $\sin \varphi = (\omega_{RF} - \Delta\omega)/\omega_L$. In this case, the beatnote is locked to the injected RF signal and changes with it. When the condition $|\omega_{RF} - \Delta\omega| > \omega_L$ is satisfied, Equation (6) will fall out of the locking range and the beatnote will no long be equal to the external modulation frequency. For mode-locking a QCL, the injected RF frequency and power has to satisfy the locking conditions given above.

Direct RF modulation was firstly introduced to THz QCL community in 2007 by Barbieri et al. [55]. They modulated the bias current that was injected into a THz QCL and observed the appearance of sideband modes in the emission spectrum, with a spacing that could be continuously tuned up to 13 GHz. The most important phenomena observed in the experiment was that when the modulation frequency approached the round-trip frequency of photons circulating in the resonant cavity, the number of QCL sidebands was considerably increased. This phenomenon, already observed in traditional lasers, was confirmed in QCL for the first time and was also in agreement with the above injection-locking theory. According to the Fourier transform, the broadened spectrum can potentially transfer to short pulses in time domain.

Thereafter, the injection locking of THz QCLs was studied in detail in the same group [54]. They investigated the longitudinal mode behavior of QCLs under different external modulation conditions. The first one was to fix the modulation frequency and change the RF modulation power. The second one was to fix the modulation power and change the modulation frequency. In both cases, a clear frequency "pulling effect" was observed as given in Ref [54]. They found a square-root dependence of the locking range with RF-power in agreement with classical injection-locking theory, as given in Equation (6). This THz QCL showed a locking range above 200 MHz, also in agreement with the theory described by Equation (7).

Then, injection locking and harmonic injection locking were also demonstrated in mid-infrared QCL through direct microwave modulation [56,57]. As shown in the light-current-voltage (LIV) curve and the spectrum in Figure 2a,c, the QCL with a broadband emission spectrum spanning 8.0– $8.6~\mu m$ is capable of delivering high optical power of over 2 W from a single facet in CW operation at approximately room temperature. Figure 2b also gives the scanning electron microscope (SEM) image of the high-power long-wave infrared QCL. Figure 2d shows the evolution of the beatnote (continuous branch) of the QCL as

current-voltage (LIV) curve and the spectrum in Figure 2a, c, the QCL with a broadband emission spectrum spanning 8.0–8.6 µm is capable of delivering high optical power of over 2 W from a single facet in CW operation at approximately room temperature. Figure 2b also gives the scanning electron microscope (SEM) image of the high-power long-waxeds infrared QCL. Figure 2d shows the evolution of the beatnote (continuous branch) of the QCL as a function of the injected RF frequency (discrete branch). Figure 2e shows the beathote frequency freq

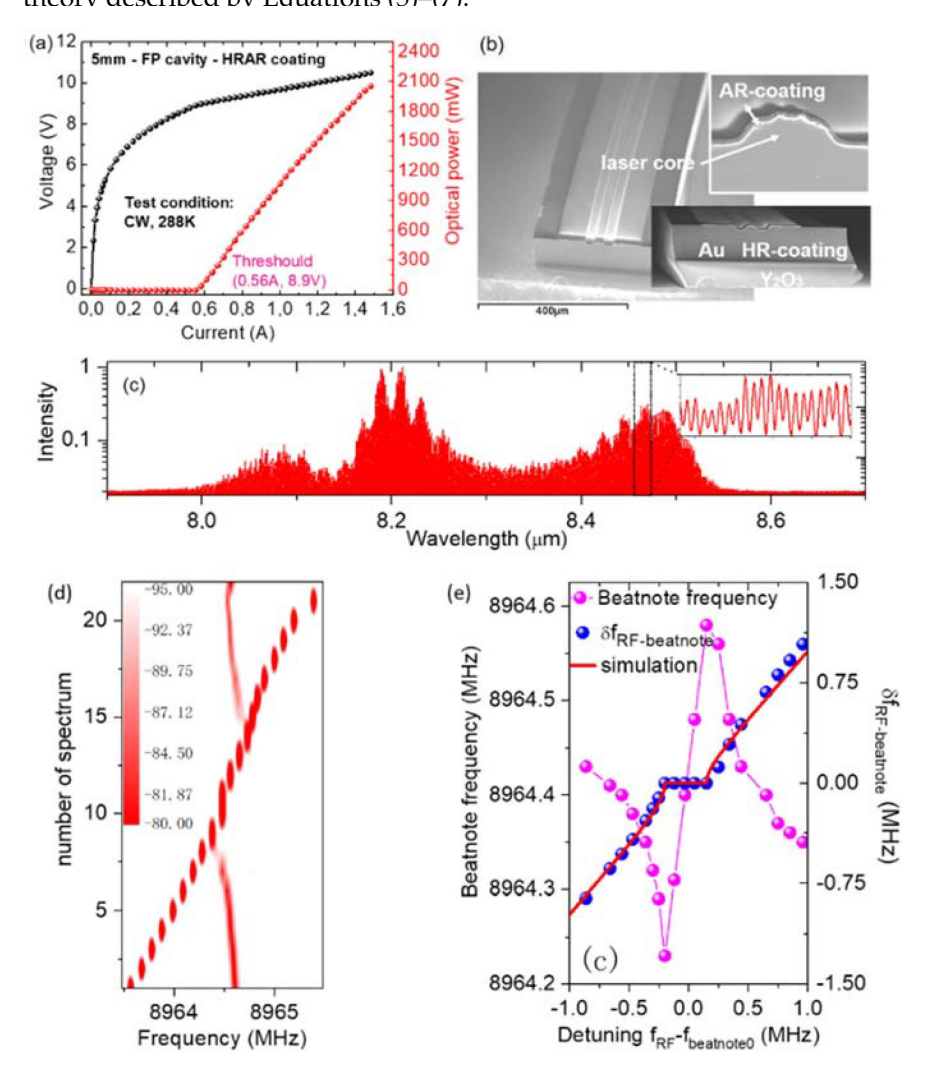


Figure 2.(4) The light-amount onlige (LIV) converse a quantum assed dose operating a troom temperature in continuous wave (b) The examing electromic assed dose operating a troom consider the permitted of the p

4. Mode-Locked THz QCLs

The class of laser is the dominating factor regarding its transient behavior that determines how it generates short pulses. For QCL, the photon lifetime (τ_{cav}) in laser cavity is in the order of magnitude 100–200 ps, while the lifetime of electrons (τ) on excited energy levels is in the order of a few picoseconds. This condition ($\tau_{cav} >> \tau$) gives an exponential growth transient behavior in the switched-on dynamic regime of QCL. Hence, QCLs

Micromachines 2022, 13, 2063

The class of laser is the dominating factor regarding its transient behavior that determines how it generates short pulses. For QCL, the photon lifetime (τ_{cav}) in laser cavity is in the order of magnitude 100–200 ps, while the lifetime of electrons (τ) on excited energy levels is in the order of a few picoseconds. This condition ($\tau_{cav} \gg \tau$) gives an exponential growth transient behavior in the switched-on dynamic regime of QCL. Hence, QCLs are class-A lasers, which theoretically presents a difficulty for ultrafast pulse generation through the Q-switch technique. Mode-locking is, therefore, the only possible choice to generate ultrafast light pulses from QCLs.

are classed losering visial wider tiseal tearning to deficiently full although the essentially the propagate in operation, therefore, the only possible choice to generate that can be amplified and propagate in its cavity, as schematically illustrated in Figure 3 (green waves). These frequencies are called longitudinal modes of a laser, which the definition of the laser. If all the modes of a laser, which are in phase and the mode spacing between these modes is identical, the electric field of all these modes will interfere constructively. This will result in an ultra-short and intense are determined by the cavity length and the active medium of the laser. If all the modes are determined by the cavity length and the second modes is identical, the electric field of all these modes will interfere constructively. This will result in an ultra-short and intense are determined by the cavity length and the active medium of the laser. If all the modes are determined by the cavity length and the active medium of the laser. If all the modes are determined by the cavity length and the active medium of the laser. If all the modes are determined by the cavity length and the active medium of the laser. If all the modes are in phase and then be partially coupled out from the cavity mirrors at every round-trip time in phase modes, will interfere constructively. This will result in an ultra-short and intense time. Temporally, a train of pulses separated by the laser cavity round-frip time will be pulse (red in Figure 3 below) in the laser cavity, it will propagate back and forth within the bottained. This is the so-called mode-locking: to put all the longitudinal modes in phase (i.e., equal mode-locking to pulses separated by the laser cavity round-trip time will be obtained. This is the so-called mode-locking: to put all the longitudinal modes in phase (i.e., equal mode-locking to pulses separated by the laser cavity round-trip time will be obtained.

Longitudinal modes in FP cavity

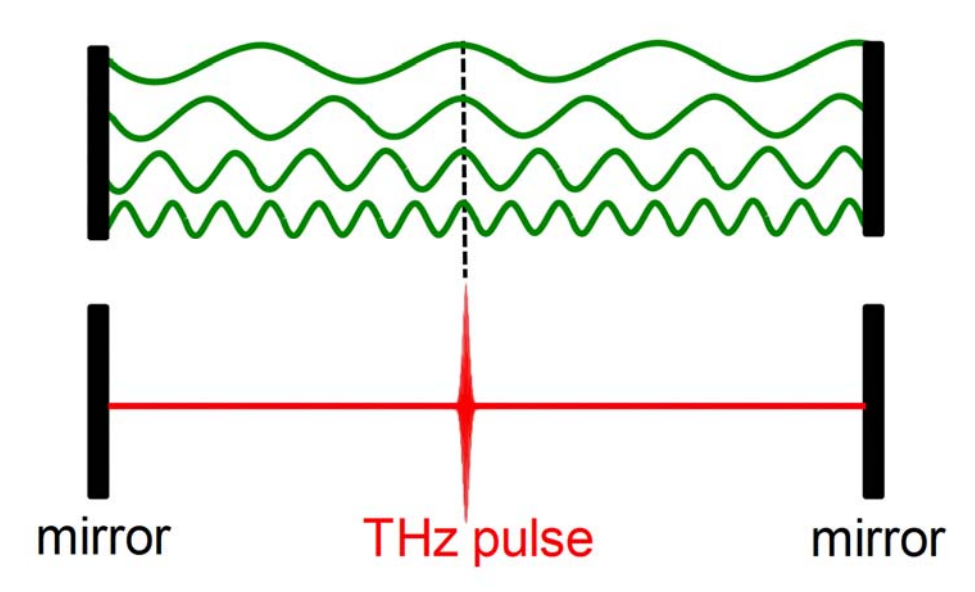


Figure 3. Schematic diagram of mode-locking in time or space domain in a Fabry-Pérot cavity. **Figure 3.** Schematic diagram of mode-locking in time or space domain in a Fabry-Pérot cavity.

If we suppose that the electric field of one longitudinal mode, for example the m^{th} one, If $w_{e}(t)$ properties field of one longitudinal mode, for example the m^{th} one, If $w_{e}(t)$ properties field of the electric field of electric fields of all these resonant modes together will give us the laser emission in the time domain:

modes together will give us the laser emission in the time domain:
$$E(t) = \sum_{1}^{m} E_m(t) = \sum_{1}^{m} A_m e^{2\pi i (f'_m t + \phi_m)} + c.c$$

$$= \sum_{1}^{m} A_m e^{i[2\pi (f_0 + m \cdot \delta f + \Delta f_m)t + \phi_m]} + c.c$$

$$= \sum_{1}^{m} A_m e^{i[2\pi (f_0 + m \cdot \delta f)t + \phi_m + 2\pi \cdot \Delta f_m \cdot t]} + c.c$$

$$= \sum_{1}^{m} A_m e^{i[2\pi (f_0 + m \cdot \delta f)t + \Phi_m(t)]} + c.c$$
(8)

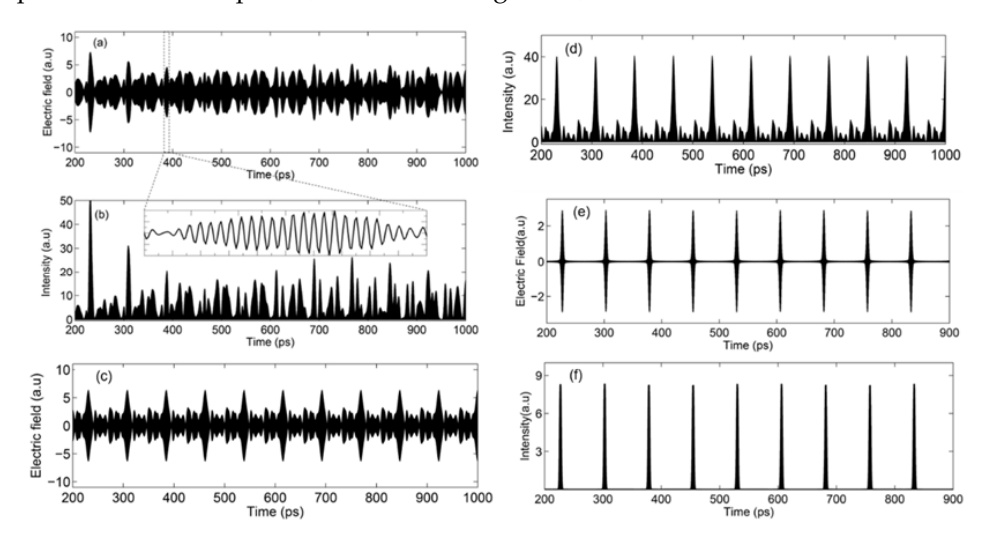
where A_m , f_m and ϕ_m are, respectively, the amplitude, frequency, and time-independent phase of the m^{th} mode. $\delta \omega$ and $\Delta \omega_m$ are, respectively, the cold cavity mode spacing and the frequency-dependent mode shifting induced by hot cavity. $\Phi_m = 2\pi \Delta f_m t + \phi_m$ is the time-dependent phase of the m^{th} mode and ϕ_m is the time-independent phase of the m^{th} mode.

$$= \sum_{i}^{m} A_{m} e^{i[2\pi(f_{0}+m\cdot\delta f)t+\Phi_{m}(t)]} + c.c$$

8 of 18

where A_m , f_m and ϕ_m are, respectively, the amplitude, frequency, and time-independent phase of the m^{th} mode. $\delta \omega$ and $\Delta \omega_m$ are, respectively, the cold cavity mode spacing and the frequency-dependent mode shifting induced by hot cavity. $\Phi_m = 2\pi \Delta f_m t + \phi_m$ is the time-dependent phase of the m^{th} mode and ϕ_m is the time-independent phase of the

mth production of the electric field. When the electric field. When the electric field. When the electric field will first electric field. When the electric field will first electric field will first electric field. When the electric field will first electric field will first electric field. When the electric field will first electric field will first electric field. When the electric field will first electric field will be f



As discussed above, the key mission of mode-locking is to remove or fix the time dependentisphase denhand, that the mission paring add-phasing is beer unby identical the time dependent phase term and make the mode spacing and phase of a laser to be identical. Generally, when a laser is mode-locked and periodic pulses are generated, δf and ϕ_m will be automatically fixed due to the "phase-matched" modulation imposed on these modes.

How can we fix the free spectral range δf of a laser and keep the modes in phase? There are many ways that can be used to achieve this, including active mode-locking, passive mode-locking and hybrid mode-locking. Each type of mode-locking can be also realized by many different detailed techniques, such as direct current modulation [58], acoustic-optic modulation [59], saturable absorption [60], and nonlinear Kerr effect [61], etc.

Here we present active mode-locking as it is the most adapted for pulse generation from QCLs. Generally, we employ an electrical modulation ω_M , which is monochromatic and very close to the mode spacing $\delta\omega$, to modulate a laser directly (i.e., modulation at the round trip of the cavity). Firstly, let us consider the modulation effect on the frequency ω_m , as is illustrated in Figure 5a. Before modulation is applied, the free-running emission mode spacings are not identical $\delta\omega_m \neq \delta\omega_{m+1}$. When modulation is applied, the central frequency ω_m will transfer a part of its energies to its modulated sidebands ($\omega_m + \omega_M$, $\omega_m - \omega_M$) and will be close in frequency to the two free-running modes (ω_{m-1} , ω_{m+1}) of the cavity. If the modulation power is strong enough, it will force the free-running frequencies (ω_{m-1} , ω_{m+1}) to move towards the sidebands' frequencies positions at ($\omega_m + \omega_M$, $\omega_m - \omega_M$) until they totally overlap $\omega_{m-1} = \omega_m - \omega_M$, $\omega_{m+1} = \omega_m + \omega_M$. Finally, the mode spacing will be locked to the modulation frequency $\delta\omega_m = \delta\omega_{m+1} = \omega_M$, as presented in Figure 5b.

 ω_m , as is illustrated in Figure 5a. Before modulation is applied, the free-running emission mode spacings are not identical $\delta\omega_m \neq \delta\omega_{m+1}$. When modulation is applied, the central frequency ω_m will transfer a part of its energies to its modulated sidebands ($\omega_m + \omega_M$, $\omega_m - \omega_M$) and will be close in frequency to the two free-running modes (ω_{m-1} , ω_{m+1}) of the cavity. If the modulation power is strong enough, it will force the free-running frequencies (ω_{m-1} , ω_{m+1}) to move towards the sidebands' frequencies positions at ($\omega_m + \omega_M$, $\omega_m - \omega_M$) until they totally overlap $\omega_{m-1} = \omega_m - \omega_M$, $\omega_{m+1} = \omega_m + \omega_M$. Finally, the mode spacing will be locked to the modulation frequency $\delta\omega_m = \delta\omega_{m+1} = \omega_M$, as presented in Figure 5b.

9 of 18

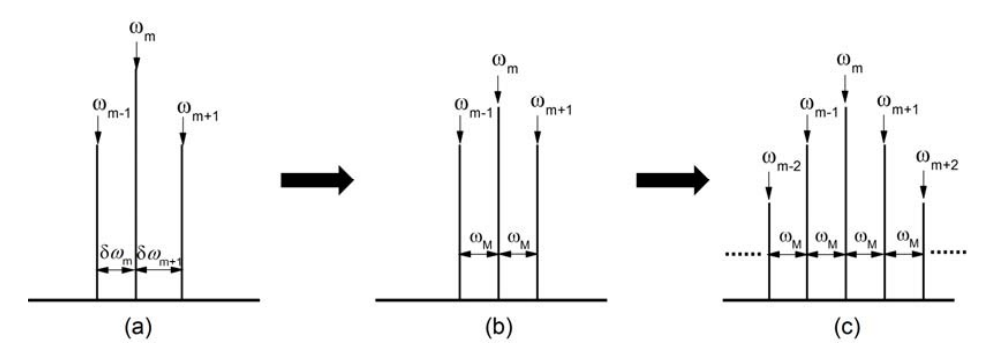


Figure 5. Schwatindia rap and the divactive chocking the first industry of Spectrum of freening emission. (b) Modulation is applied on a laser (c) Laser is mode-locked.

Tunning emission. (b) Modulation is applied on a laser. (c) Laser is mode-locked.

Above we have analyzed the modulation effect only on the central frequency ω_m . We can analyze the other frequencies in the same way: ω_{m-1} to obtain $\delta\omega_{m-2}=\delta\omega_{m}=\omega_{m}$, ω_{m-2} to obtain $\delta\omega_{m-2}=\delta\omega_{m}=\omega_{m}$, $\omega_{m-2}=\delta\omega_{m}=\omega_{m}$, at the end, we have $\delta\omega_{m-2}=\delta\omega_{m}=\omega_{m}$, the end of $\delta\omega_{m-2}=\delta\omega_{m}=\omega_{m}$, $\omega_{m-2}=\delta\omega_{m}=\omega_{m}$, $\omega_{m-2}=\delta\omega_{m}=\omega_{m}$, $\omega_{m-2}=\delta\omega_{m}=\omega_{m}$, $\omega_{m-2}=\delta\omega_{m}=\omega_{m}$, at the end, we have $\delta\omega_{m-2}=\delta\omega_{m}=\omega_{m}$, the end of $\delta\omega_{m-1}=\delta\omega_{m}=\omega_{m}$, $\omega_{m-2}=\delta\omega_{m}=\omega_{m}$. At the end, we have $\delta\omega_{m-2}=\delta\omega_{m}=\omega_{m}$, the end of $\delta\omega_{m-1}=\delta\omega_{m}=\omega_{m}$, $\omega_{m-2}=\delta\omega_{m}=\omega_{m}$, $\omega_{m}=\omega_{m}=\omega_{m}$, $\omega_{m}=\omega_{m}=\omega_{m}$, $\omega_{m}=\omega_{m}=\omega_{m}$, $\omega_{m}=\omega_{m}=\omega_{m}=\omega_{m}$, $\omega_{m}=\omega_{$

tum Whitke At manifonal Symition lades of fast each the CVCV. Time stiders all mass place between thorter than in interband lasers [19-21,23], and a time considerably shorter than the phoelectrons ton round-trip cavity time. This is believed to prevent these devices from being modein quantum wells. As mention above, this leads to fast gain recovery time, orders of locked (multiple pulses are generated within the CCL cavity) and, thus, unable to generate magnitude shorter than in interband lasers [19-21,23], and a time considerably shorter than attended to prove the photoevery in the street approaches.

However, it has been shown recently that these devices can be actively mode-locked, where the QCL is modulated at microwave frequencies, to generate a train of picosecond pulses [22,62]. The key to these demonstrations has been the development of new ultrafast techniques for the THz range. In the first case, detection of the emitted pulse train has been made possible by phase-locking the QCL repetition rate and carrier frequency to a high order harmonic of the repetition rate of a mode-locked femtosecond laser. This technique permits coherent detection of the THz electric field, and allows the control of the carrier-envelope phase shift of the QCL. Its disadvantage is that it undersamples the electric field of the pulse train of lasers in the time domain.

An alternative ultrafast detection technique called the "injection seeding technique" has also been developed [63]. This technique has the full capability to measure all the information of QCL emission in time domain, including phase, amplitude, intensity, spectrum, and full electric field, as shown in Figure 6. This provides the possibility to observe directly pulse-train generation and has paved the way for QCL mode-locking demonstration directly in time domain.

Immediately after the development of this injection seeding technique, mode-locking of THz QCLs was realized and demonstrated in time domain [32–34,64]. A series of important work was published on this research topic, showing that THz QCLs could be mode-locked for short pulse generation. Figure 7a shows the THz intensity emitted by an actively mode-locked QCLs over picosecond time scales (without a seed). Both the initiation of mode-locked pulses and the steady-state regime were examined. For bias conditions well above threshold, a sinusoidal modulation of the emission was achieved; however, when the QCL was biased around threshold and the round-trip modulation was strong, Gaussian-shaped transform limited mode-locked pulses with a full width at half

pulses [22,62]. The key to these demonstrations has been the development of new ultrafast techniques for the THz range. In the first case, detection of the emitted pulse train has been made possible by phase-locking the QCL repetition rate and carrier frequency to a high order harmonic of the repetition rate of a mode-locked femtosecond laser. This technique permits coherent detection of the THz electric field, and allows the control of the maximum (Flyfely) hase show were observed. Figure altabet useful field in the short show the property of the figure and without round-trip modulation, respectively in the time domain the injection and the training two manufactors are the people of the repetition of the synchrolic parameter of the property of the remaining the parameter of the property of the people of the parameter of the parameter of the property of the parameter of the parameter of the parameter of the property of the parameter of the property of the parameter of the param

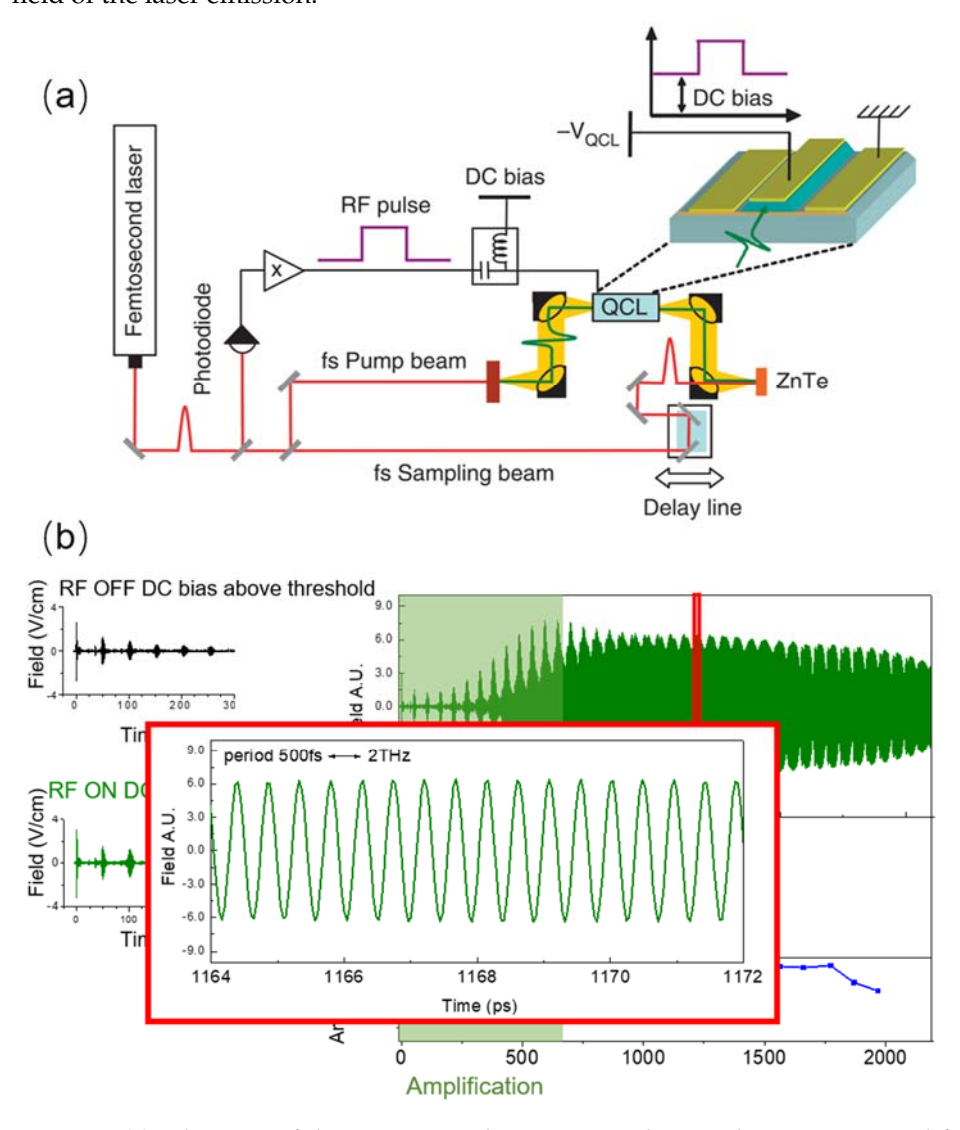


Figure 6. (a) Schematic of the exponimental cripture Retrospositives a general red from a power Reputation of the processor of the exponimental criptures. The Reputation of the processor of the red from the Reputation of the pulses are completely influminating a biased introdigitated automna within a remanescend pump beam. The Thap these are coupled into a fract of the QCL with parabolic mirrors. The QCL output field from the other facet is measured using electro-optic sampling in a ZnTe-crystal with a fem to second sampling. (b) The experimental result: full electric field resolved emission of a THz QCL working at 2 THz. (Figure (a) from Ref [63], licensed under a Creative Commons Public (CCPL) license).

relied on synchronizing the mode-locked pulses to a reference laser and was applied to 15-ps pulses generated by a 2-THz QCL. The pulses from the actively mode-locked laser were completely characterized in field and in time with a sub-ps resolution, allowing us to determine the amplitude and phase of each cavity mode. Figure 7c shows the zoom in of a light pulse from the mode-locked QCL. We can clearly resolve the oscillation of the electric field of the laser emission.

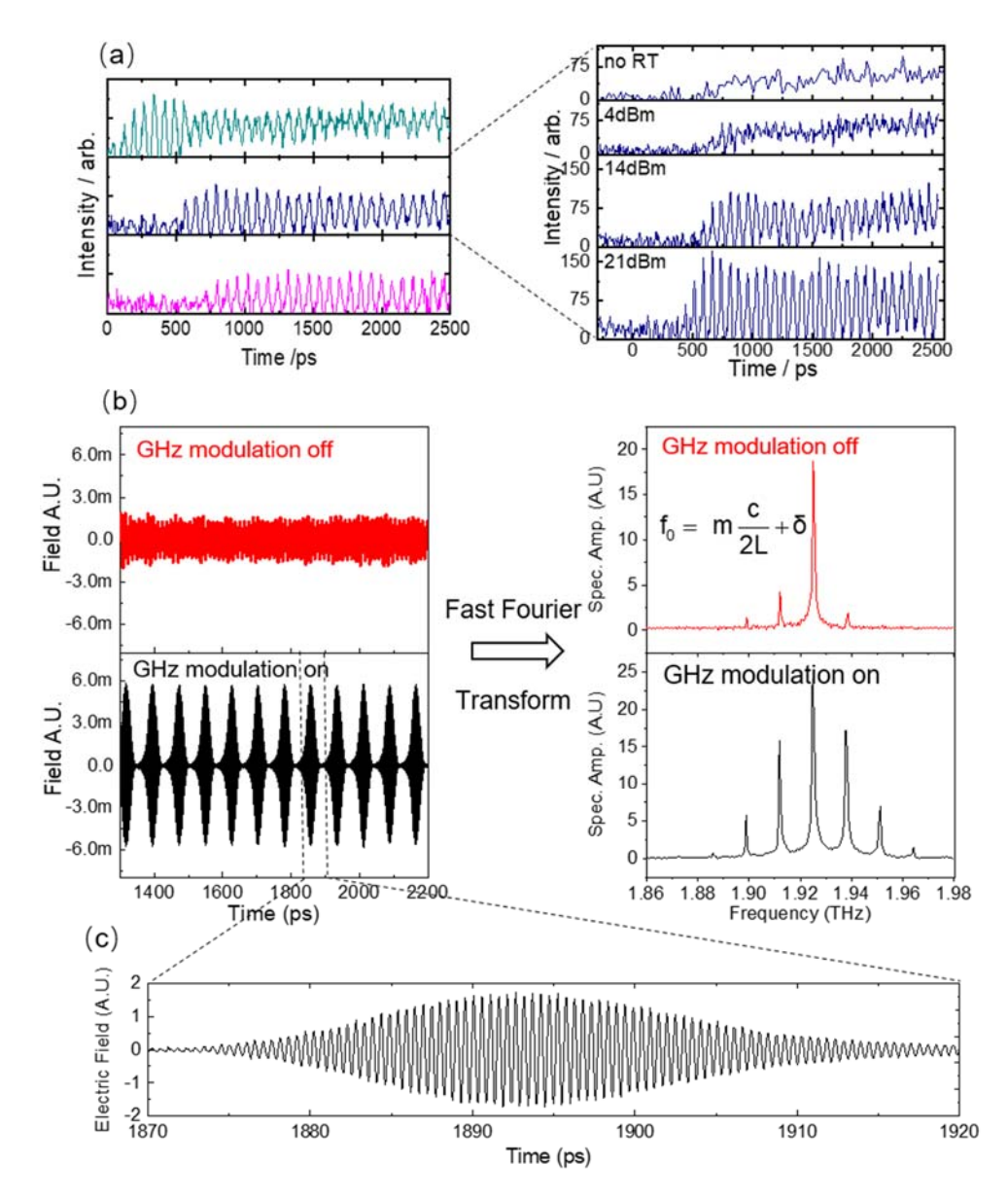
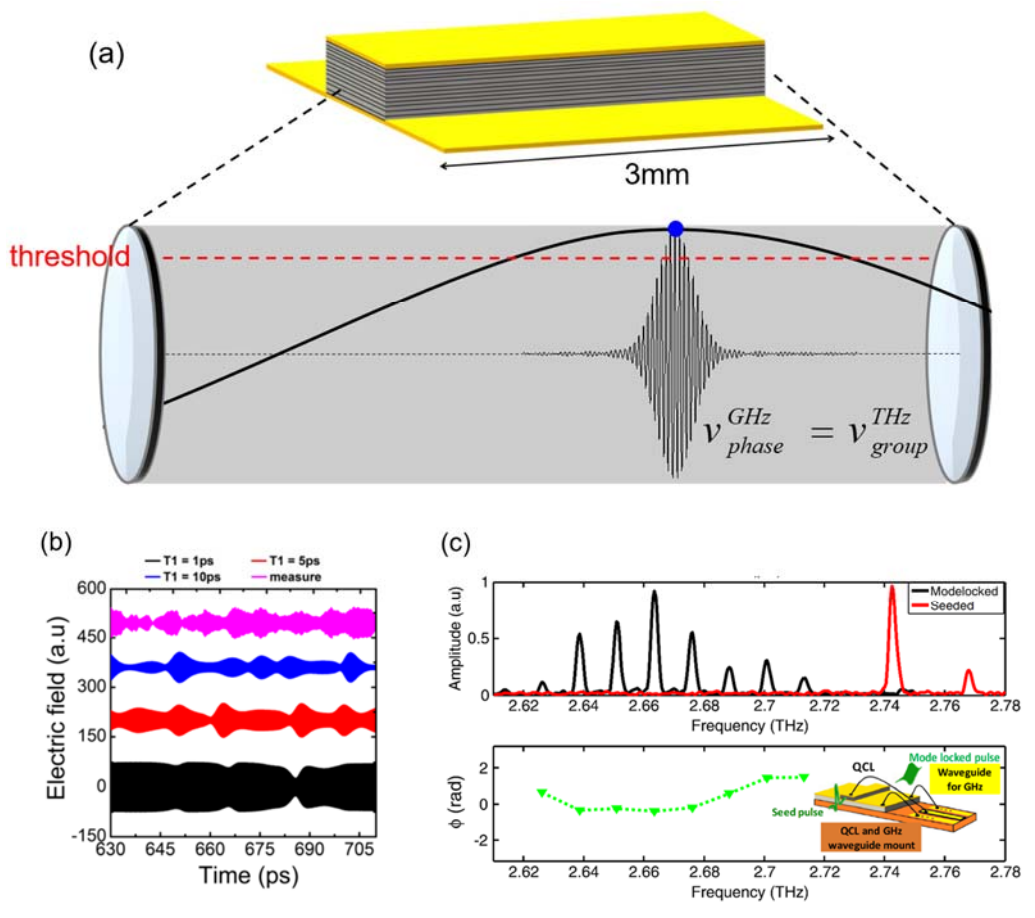


Figure 7. (a) Sampled THz intensity from the QCL. Left: at different currents. Right: a different modulation power. The detailed explanation on different color can be found in Ref [32] (b) The electric field (left) and its corresponding spectra (right) of QCL emission with and without round-trip modulation, respectively. (c) The zoom in of one THz pulse of QCL emission. (Figure (a) from Ref [32], reprint with the permission of AIP Publishing).

Since then, mode-locked THz QCLs have been experimentally demonstrated using different detection approaches as discussed above. However, the exact mechanism of mode-locking in QCLs is still unknown, which strongly limits new avenues to be explored to generate shorter and more intense laser pulses. Over a series of samples and measurements by researchers [23], it has been found that, contrary to a long-standing belief that the QCL gain dynamics are the limiting factor, the key mechanism is in fact a nonlinear interaction between the pulse generated and the applied electrical modulation [23], as shown in Figure 8a. This is important information and has permitted new avenues to be explored to generate shorter and intense pulses.

to generate shorter and more intense laser pulses. Over a series of samples and measurements by researchers [23], it has been found that, contrary to a long-standing belief that the QCL gain dynamics are the limiting factor, the key mechanism is in fact a nonlinear interaction between the pulse generated and the applied electrical modulation [23], as shown in Figure 8a. This is important information and has permitted new avenues to be explored to generate shorter and intense pulses.



Higures8(4) The cohematics of model deining extentions of COC(b) The The Menthalle Biolasimona-diene of the gather every cineal field while deining profile and the configuration of a seeded for the corresponds to experimental data. (c) Top: the spectra of a seeded (red) and a modelocked (black) OCL, bottom: the phases of the eight modelocked longitudinal modes (green triandlack) OCL, bottom: the phases of the eight modelocked longitudinal modes (green triandlack) OCL, bottom: the phases of the eight modelocked longitudinal modes (green triandlack) OCL, bottom: the phases of the eight modelocked longitudinal modes (green triandlack) OCL, bottom: the phases of the eight modelocked longitudinal modes (green triandlack) OCL, bottom: the phases of the eight modelocked longitudinal modes (green triandlack) OCL, bottom: the phases of the eight modelocked longitudinal modes (green triandlack) OCL, bottom: the phases of the eight modelocked longitudinal modes (green triangles). Inset: OCL schematic showing the device integrated with a microwave waveguide for active of the phases of the eight modelocked longitudinal modes (green triangles). Inset: OCL schematic showing the device integrated with a microwave waveguide for active of the phases of the eight modelocked longitudinal modes (green triangles). Inset: OCL schematic showing the device integrated with a microwave waveguide for active of the phases of the eight modelocked longitudinal modes (green triangles). Inset: OCL schematic showing the device integrated with a microwave waveguide for active of the phases of the eight modelocked longitudinal modes (green triangles). Inset: OCL schematic showing the device integrated with a microwave waveguide for active of the phases of the eight modelocked longitudinal modes (green triangles). Inset: OCL schematic showing the device integrated with a microwave waveguide for active of the phases of the eight modelocked longitudinal modes (green triangles). Inset: OCL schematic showing the device integrated with a microwave wave

Figure 8b shows the Maxwell-Bloch simulations of the gain recovery time (T1). It was Figure 8b shows the Maxwell-Bloch simulations of the gain recovery time (T1). It was calculated using Maxwell-Bloch finite-difference time-domain simulations in a two-level was calculated using Maxwell-Bloch finite-difference time-domain simulations in a two-system [23]. The procedure is detailed in depth in Ref. [31]. Here, a dephasing time about 9.6 ps from the full-width at half-maximum of the gain and a total waveguide loss of 12 cm⁻¹ from the first pass gain measurements of the longitudinal optical (LO) phonon-depopulation-based QCL were used. A time data with a gain recovery time of ~5 ps showed the best 'fit' with the data. The ultrafast gain recovery time measured here, which did not limit pulse generation, could be used as an advantage to generate more intense and shorter pulses if short intense electrical pulses could be used. Although difficult to generate electronically, optically generated electrical pulses using ultrafast lasers combined with ultrafast materials are feasible and these could then be used to switch the QCL on sub-picosecond time scales. Further techniques that could circumvent the current limitations would be the application of greater microwave power for higher pulse energies and the application of hybrid mode-locking techniques to shorten the pulses to sub-10 ps values. Figure 8c top shows the spectra of a seeded (red) and a mode-locked (black) QCL; bottom shows the phases of the eight mode-locked longitudinal modes (green triangles).

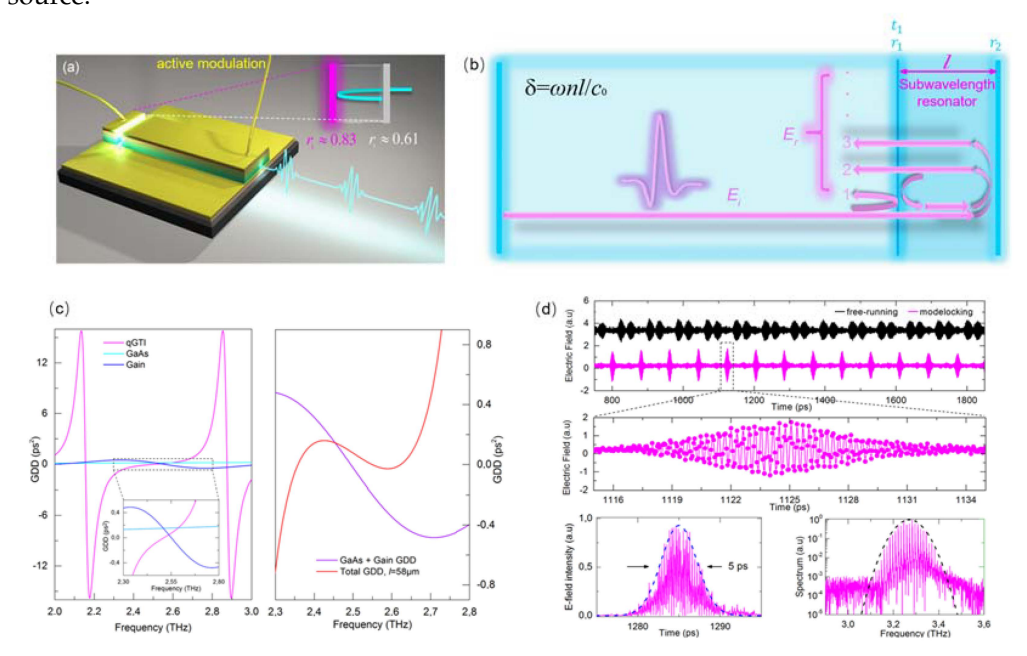
Micromachines 2022, 13, 2063 13 of 18

5. Pulse Shortening in Mode-Locked THz QCLs

As of 2013, active mode-locked THz QCLs have been demonstrated through different measures in different groups. However, the pulse width of mode-locked QCLs is quite large, falling between 10 and 20 ps. Researchers have attempted many different approaches, including using broad-bandwidth QCLs, designing different geometry structures, adopting hybrid mode-locking techniques, etc., to compress the pulse width below 10 ps but without any success despite many active research efforts [54,56,57,65].

In 2016, the research group at TU Wien Vienna showed that a single THz pulses as short as 2.5 ps could be generated from a QCL [66]. However, this was not a train of pulses, with subsequent pulses broadening as the QCL was not actively mode-locked.

To realize a mode-locked pulse train, a monolithic on-chip dispersion compensation scheme to shorten the THz pulses of mode-locked QCLs was proposed [26]. This was based on the realization of a small coupled cavity resonator that acted as an 'off resonance' Gires—Tournois interferometer (GTI), permitting large THz spectral bandwidths to be compensated, as shown in Figure 9. In this work, the THz pulses of mode-locked QCLs was considerably shortened from 16 ps to 4 ps. This permitted the compression of THz pulses of mode-locked QCLs beyond the 10 ps barrier that had stood for several years. This result marks an important milestone in exploring ultrafast light-pulse generation Micromachines 2022, 13, × FOR PEER BENTHYOde-locked QCLs. The novel application of a GTI also opens up a direct 4 rotale to sub-picosecond and single cycle pulses in the THz range from a compact semiconductor source.



Figier 9. (4) The schematic of short-pulse seneration based on the pingline price of compensation. (b) The schematic of dispersion compensation based on Gires-Tournois Interferometer. (c) Group Delay Simulations of the gain, material and GTI, Left: The individual GDD contributions of the GTI, Delay Simulations of the gain, material and GTI, Left: The individual GDD contributions of the GTI, Delay Simulations of the gain, material and GTI Left: The individual GDD contributions of the GTI, GaAs and the QCL gain. Right: The total GDD for a 55 jum (red) length GTIs. The contribution of the GTI, GaAs and the QCL gain. Signs The total GDD for a 55 jum (red) length GTIs. The contribution of the gamental material schools are supported by the gamental contribution of the gamental material GDD for a 55 jum (red) from Ref [26], licensed under a Creative Commons Attribution (CC BY) license).

6. Pulse Generation in Mid-Infrared QCLs

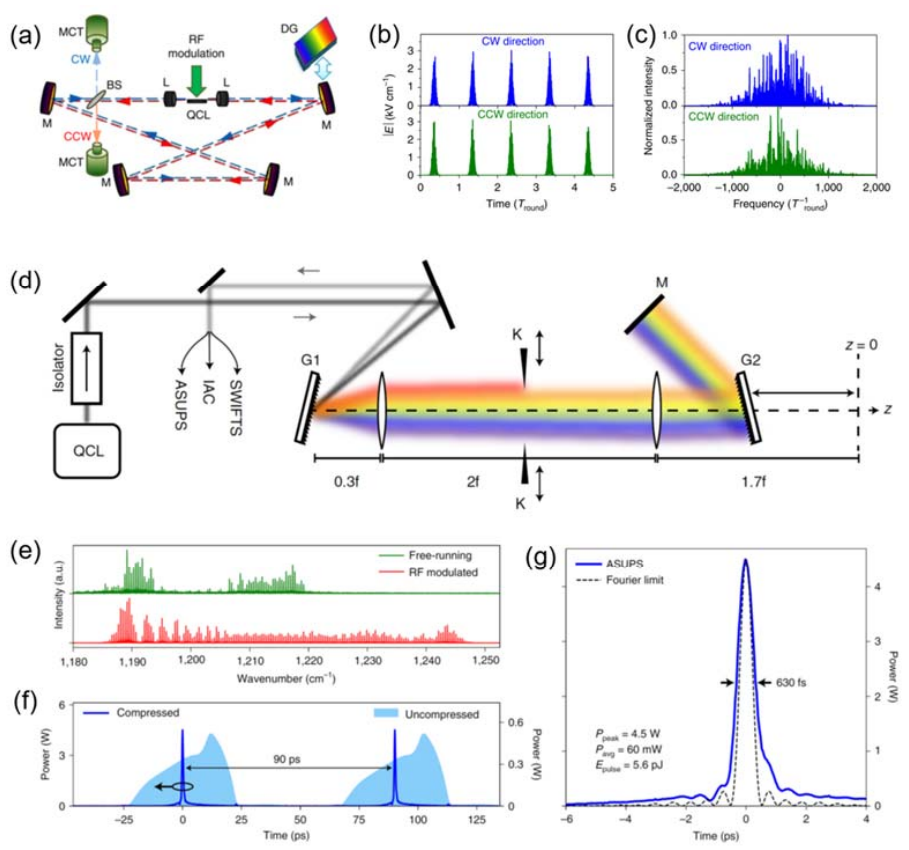
6. Pulse Generation in Mid-Infrared OCLs is far ahead of THz QCLs [3,4,6–8,67], but its mode of the generation of mid-infrared OCLs is far ahead of THz QCLs [3,4,6–8,67], but its mode of the graph of principal princi

Micromachines 2022, 13, 2063 14 of 18

in 2015 by Belyanin's group in Texas [25]. They investigated the dynamics of actively modulated mid-infrared QCLs using space- and time-domain simulations of coupled density matrix and Maxwell equations, with resonant tunneling current taken into account. They showed that it was possible to achieve active mode-locking and stable generation of picosecond pulses in QCLs by bias modulation of a short section of a monolithic Fabry–Pérot cavity.

In the same year, active mode-locking of mid-infrared QCLs at a wavelength of 5 µm was experimentally demonstrated in a free-space external ring cavity QCL, as shown in Figure 10a [24]. The laser operated at room temperature and stayed in mode-locking state over the full dynamic range of injection currents. Figure 10b,c shows the estimated pulse width and corresponding spectra using a four-subband model for the QCL active region, which ranges between 10 ps and 45 ps depending on the cavity length. In the paper, the theoretical modeling showed that one could achieve much shorter pulses and broader phase-locked frequency combs by modulating the pumping with shorter and sharper pulses winstead of the sinusoidal modulation. This finding is completely in agreement with

Micromachines 2022, 13, x FOR PEER**puilses** winstead of the sinusoidal modulation. This finding is completely in agreement with the experimental observation in Ref. [23].



Higure 10. (a) Optical sectupe of free espace exact mind anyty quantum classer Basen BS: beam splitter; CCW confirted choices direction; Cow via chosen decinification and the individual of the leaver of the electric fields and (c) their specific lenses; M: mirrors; MCT: detector, (b) Absolute values of the electric fields and (c) their specific lenses; M: mirrors in or a simusoidal modulation of bias with the modulation period equal to 1.01 fround. (d) The experimental scitus of the electric fields and (c) their specific region as a simusoidal modulation of bias with the modulation period equal to 1.01 fround. (d) The experimental scitus of the electric fields and (c) their specific for a scitus of the experimental scitus of the experimenta

beatnote interferometry, and interferometric autocorrelation. Figure 10e shows the free-

Micromachines 2022, 13, 2063 15 of 18

Recently, Faist's group at ETH Zurich also demonstrated an approach capable of producing near-transform-limited sub-picosecond pulses (630 femtosecond) with several watts of peak power at a wavelength of around 8µm using a diffraction grating compressor, as shown in Figure 10d [27]. Starting from a frequency-modulated phase-locked state, ultrashort high-peak-power pulses were generated via spectral filtering, gain modulation-induced spectral broadening, and external-pulse compression. They investigated the pulse width of QCLs emission using a novel asynchronous sampling method, coherent beatnote interferometry, and interferometric autocorrelation. Figure 10e shows the free-running and round-trip-modulated optical spectra, respectively. It can be clearly observed that a considerable increase in spectral bandwidth has been achieved in the latter case. Such a temporal modulation brings a strong overall amplitude modulation, accomplished with the decrease of emitted average power due to increased gain saturation, as shown in Figure 10f. This is another milestone in ultrafast pulse generation from QCLs following the 4 ps THz pulse generation from mode-locked THz QCLs. These achievements presented above are also listed in Table 1 given below:

	Pulse Width	Wavelength/ Frequency	Operation Tempera- ture	Method	Peak Power	
2009 Ref. [62]	3 ps	6.3 μm	77 K	active modulation	0.5 pJ	
2011 Ref. [22]	10 ps	2.5 THz	20 K	coherent sampling	×	
2012 Refs. [32–34]	10–20 ps	2 THz	10 K	active modulation	×	
2016 Ref. [24]	10–45 ps	5.25 μm	300 K	external cavity	12 mW	
2017 Ref. [26]	4 ps	2.2–2.8 THz	20 K	dispersion compensation	×	
2021 Ref. [27]	0.63 ps	8 μm	300 K	external pulse compression	4.5 W	

Table 1. Achievements on pulse generation from QCLs.

7. Conclusions and Perspectives

To conclude, pulse generation through mode-locking of QCLs has undergone considerable development in the past decade. Owing to the fast dynamics, QCLs were thought to be very difficult to mode-lock. Through active mode-locking and pulse compression, an ultrashort pulse train as short as 4 ps in THz and 0.6 ps in mid-infrared regime has been realized from mode-locked QCLs. These results push QCLs to a new milestone, enabling a range of applications in fundamental research, high-tech industry and defense technology, particularly in mid-infrared and THz nonlinear optics where high pulse energies are typically required. With further development of this technology, many new QCL-based applications will emerge in the near future, potentially replacing or being complementary to OPA technologies.

Author Contributions: F.W. organized the manuscript preparation of the review paper. Z.C. and F.W. prepared the initial draft. X.Q. prepared the "ultrafast dynamics of QCL" section. M.R. and S.D. revised and improved the whole paper. All authors have read and agreed to the published version of the manuscript.

Funding: The authors acknowledge startup funding from the Shenzhen Institute for Quantum Science and Engineering, Southern University of Science and Technology, the International Quantum Academy, the funding from European Union under the Horizon 2020 research and innovation programs FET-Open grant EXTREME-IR 964735, the French National Research Agency (ANR-18-CE24-0013-02-"TERASEL"), Australian Research Council Discovery Project (DP160103910 and DP200101948), National Science Foundation-"Room temperature high-power terahertz semiconductor laser with high-quality beam shape and stable spectral emission" Grant # 2149908. X.Q. acknowledges support under the Advance Queensland Industry Research Fellowships program.

Conflicts of Interest: The authors declare no conflict of interest.

Micromachines **2022**, 13, 2063 16 of 18

References

1. Faist, J.; Capasso, F.; Sivco, D.; Sirtori, C.; Hutchinson, A.; Cho, A.Y. Quantum Cascade Laser. *Science* 1994, 264, 553–556. [CrossRef] [PubMed]

- 2. Köhler, R.; Tredicucci, A.; Beltram, F.; Beere, H.E.; Linfield, E.; Davies, A.G.; Ritchie, D.; Iotti, R.C.; Rossi, F. Terahertz Semiconductor-Heterostructure Laser. *Nature* 2002, 417, 156–159. [CrossRef] [PubMed]
- 3. Razeghi, M. High-Performance InP-Based Mid-IR Quantum Cascade Lasers. *IEEE J. Select. Topics Quantum Electron.* **2009**, 15, 941–951. [CrossRef]
- 4. Wang, F.; Slivken, S.; Wu, D.H.; Lu, Q.Y.; Razeghi, M. Continuous wave quantum cascade lasers with 5.6 W output power at room temperature and 41% wall-plug efficiency in cryogenic operation. *AIP Adv.* **2020**, *10*, 055120. [CrossRef]
- 5. Bai, Y.; Bandyopadhyay, N.; Tsao, S.; Slivken, S.; Razeghi, M. Room temperature quantum cascade lasers with 27% wall plug efficiency. *Appl. Phys. Lett.* **2011**, *98*, 181102. [CrossRef]
- 6. Wang, F.; Slivken, S.; Wu, D.H.; Razeghi, M. Room temperature quantum cascade lasers with 22% wall plug efficiency in continuous-wave operation. *Opt. Express* **2020**, *28*, 17532–17538. [CrossRef] [PubMed]
- 7. Wang, F.; Slivken, S.; Wu, D.H.; Razeghi, M. Room temperature quantum cascade laser with ~31% wall-plug efficiency. *AIP Adv.* **2020**, *10*, 075012. [CrossRef]
- 8. Wang, F.; Slivken, S.; Razeghi, M. High-brightness LWIR quantum cascade lasers. Opt. Lett. 2021, 46, 5193. [CrossRef]
- 9. Li, L.; Chen, L.; Zhu, J.; Freeman, J.; Dean, P.; Valavanis, A.; Davies, A.; Linfield, E. Terahertz quantum cascade lasers with >1 W output powers. *Electron. Lett.* **2014**, *50*, 309–311. [CrossRef]
- 10. Wang, F.; Kundu, I.; Chen, L.; Li, L.; Linfield, E.H.; Davies, A.G.; Moumdji, S.; Colombelli, R.; Mangeney, J.; Tignon, J.; et al. Engineered far-fields of metal-metal terahertz quantum cascade lasers with integrated planar horn structures. *Opt. Express* **2016**, 24, 2174–2182. [CrossRef]
- 11. Vitiello, M.S.; Consolino, L.; Bartalini, S.; Taschin, A.; Tredicucci, A.; Inguscio, M.; De Natale, P. Quantum-limited frequency fluctuations in a terahertz laser. *Nat. Photon-* **2012**, *6*, 525–528. [CrossRef]
- 12. Burghoff, D.; Kao, T.-Y.; Han, N.; Chan, C.W.I.; Cai, X.; Yang, Y.; Hayton, D.J.; Gao, J.-R.; Reno, J.L.; Hu, Q. Terahertz laser frequency combs. *Nat. Photon.* **2014**, *8*, 462–467. [CrossRef]
- 13. Lu, Q.; Wang, F.; Wu, D.; Slivken, S.; Razeghi, M. Room temperature terahertz semiconductor frequency comb. *Nat. Commun.* **2019**, *10*, 2403. [CrossRef] [PubMed]
- 14. Haus, H.A. Mode-locking of lasers. IEEE J. Select. Topics Quantum Electron. 2000, 6, 1173–1185. [CrossRef]
- 15. Fujimoto, J.G.; Weiner, A.M.; Ippen, E.P. Generation and measurement of optical pulses as short as 16 fs. *Appl. Phys. Lett.* **1984**, 44, 832–834. [CrossRef]
- 16. Fork, R.L.; Cruz, C.B.; Becker, P.C.; Shank, C.V. Compression of optical pulses to six femtoseconds by using cubic phase compensation. *Opt. Lett.* **1987**, *12*, 483–485. [CrossRef]
- 17. Hargrove, L.E.; Fork, R.L.; Pollack, M.A. Locking of he–ne laser modes induced by synchronous intracavity modulation. *Appl. Phys. Lett.* **1964**, *5*, 4–5. [CrossRef]
- 18. DiDomenico, M. Small-Signal Analysis of Internal (Coupling-Type) Modulation of Lasers. *J. Appl. Phys.* **1964**, *35*, 2870–2876. [CrossRef]
- 19. Green, R.P.; Tredicucci, A.; Vinh, N.Q.; Murdin, B.; Pidgeon, C.; Beere, H.E.; Ritchie, D.A. Gain recovery dynamics of a terahertz quantum cascade laser. *Phys. Rev. B* **2009**, *80*, 075303. [CrossRef]
- 20. Choi, H.; Diehl, L.; Wu, Z.-K.; Giovannini, M.; Faist, J.; Capasso, F.; Norris, T.B. Gain Recovery Dynamics and Photon-Driven Transport in Quantum Cascade Lasers. *Phys. Rev. Lett.* **2008**, *100*, 167401. [CrossRef]
- 21. Bacon, D.R.; Freeman, J.R.; Mohandas, R.A.; Li, L.; Linfield, E.H.; Davies, A.G.; Dean, P. Gain recovery time in a terahertz quantum cascade laser. *Appl. Phys. Lett.* **2016**, *108*, 081104. [CrossRef]
- 22. Barbieri, S.; Ravaro, M.; Gellie, P.; Santarelli, G.; Manquest, C.; Sirtori, C.; Khanna, S.P.; Linfield, E.; Davies, A. Coherent sampling of active mode-locked terahertz quantum cascade lasers and frequency synthesis. *Nat. Photon.* **2011**, *5*, 306–313. [CrossRef]
- 23. Wang, F.; Maussang, K.; Moumdji, S.; Colombelli, R.; Freeman, J.R.; Kundu, I.; Li, L.; Linfield, E.H.; Davies, A.G.; Mangeney, J.; et al. Generating ultrafast pulses of light from quantum cascade lasers. *Optica* 2015, 2, 944–949. [CrossRef]
- 24. Revin, D.G.; Hemingway, M.; Wang, Y.; Cockburn, D.G.R.M.H.J.W.; Belyanin, Y.W.A. Active mode locking of quantum cascade lasers in an external ring cavity. *Nat. Commun.* **2016**, *7*, 11440. [CrossRef] [PubMed]
- 25. Wang, Y.; Belyanin, A. Active mode-locking of mid-infrared quantum cascade lasers with short gain recovery time. *Opt. Express* **2015**, 23, 4173–4185. [CrossRef] [PubMed]
- 26. Wang, F.; Nong, H.; Fobbe, T.; Pistore, V.; Houver, S.; Markmann, S.; Jukam, N.; Amanti, M.; Sirtori, C.; Moumdji, S.; et al. Short Terahertz Pulse Generation from a Dispersion Compensated Modelocked Semiconductor Laser. *Laser Photonics Rev.* **2017**, *11*, 1700013. [CrossRef]
- 27. Täschler, P.; Bertrand, M.; Schneider, B.; Singleton, M.; Jouy, P.; Kapsalidis, F.; Beck, M.; Faist, J. Femtosecond pulses from a mid-infrared quantum cascade laser. *Nat. Photon.* **2021**, *15*, 919–924. [CrossRef]
- 28. Wang, F.; Pistore, V.; Riesch, M.; Nong, H.; Vigneron, P.-B.; Colombelli, R.; Parillaud, O.; Mangeney, J.; Tignon, J.; Jirauschek, C.; et al. Ultrafast response of harmonic modelocked THz lasers. *Light Sci. Appl.* **2020**, *9*, 51. [CrossRef]
- 29. Kundu, I.; Wang, F.; Qi, X.; Nong, H.; Dean, P.; Freeman, J.R.; Valavanis, A.; Agnew, G.; Grier, A.T.; Taimre, T.; et al. Ultrafast switch-on dynamics of frequency-tuneable semiconductor lasers. *Nat. Commun.* **2018**, *9*, 3076. [CrossRef]

Micromachines 2022, 13, 2063 17 of 18

30. Weber, C.; Banit, F.; Butscher, S.; Knorr, A.; Wacker, A. Theory of the ultrafast nonlinear response of terahertz quantum cascade laser structures. *Appl. Phys. Lett.* **2006**, *89*, 091112. [CrossRef]

- 31. Freeman, J.R.; Maysonnave, J.; Khanna, S.; Linfield, E.H.; Davies, A.G.; Dhillon, S.S.; Tignon, J. Laser-seeding dynamics with few-cycle pulses: Maxwell-Bloch finite-difference time-domain simulations of terahertz quantum cascade lasers. *Phys. Rev. A* **2013**, *87*, 063817. [CrossRef]
- 32. Freeman, J.R.; Maysonnave, J.; Jukam, N.; Cavalié, P.; Maussang, K.; Beere, H.E.; Ritchie, D.A.; Mangeney, J.; Dhillon, S.S.; Tignon, J. Direct intensity sampling of a modelocked terahertz quantum cascade laser. *Appl. Phys. Lett.* **2012**, *101*, 181115. [CrossRef]
- 33. Freeman, J.R.; Maysonnave, J.; Beere, H.E.; Ritchie, D.A.; Tignon, J.; Dhillon, S.S. Electric field sampling of modelocked pulses from a quantum cascade laser. *Opt. Express* **2013**, *21*, 16162–16169. [CrossRef] [PubMed]
- 34. Maysonnave, J.; Maussang, K.; Freeman, J.R.; Jukam, N.; Madéo, J.; Cavalié, P.; Rungsawang, R.; Khanna, S.P.; Linfield, E.; Davies, A.; et al. Mode-locking of a terahertz laser by direct phase synchronization. *Opt. Express* **2012**, *20*, 20855–20862. [CrossRef] [PubMed]
- 35. Barbieri, S.; Gellie, P.; Santarelli, G.; Ding, L.; Maineult, W.; Sirtori, C.; Colombelli, R.; Beere, H.; Ritchie, D. Phase-locking of a 2.7-THz quantum cascade laser to a mode-locked erbium-doped fibre laser. *Nat. Photon.* **2010**, *4*, 636–640. [CrossRef]
- 36. Hugi, A.; Villares, G.; Blaser, S.; Liu, H.C.; Faist, J. Mid-infrared frequency comb based on a quantum cascade laser. *Nature* **2012**, 492, 229–233. [CrossRef]
- 37. Faist, J.; Villares, G.; Scalari, G.; Rösch, M.; Bonzon, C.; Hugi, A.; Beck, M. Quantum Cascade Laser Frequency Combs. *Nanophotonics* **2016**, *5*, 272–291. [CrossRef]
- 38. Gkortsas, V.; Gordon, A.; Jirauschek, C.; Wang, C.; Kuznetsova, L.; Diehl, L.; Belkin, M.A.; Belyanin, A.; Capasso, F.; Kartner Franz, X. Spatial Hole Burning in Actively Mode-Locked Quantum Cascade Lasers. In Proceedings of the 2009 Conference on Lasers and Electro-Optics and 2009 Conference on Quantum Electronics and Laser Science Conference, Baltimore, MD, USA, 2–4 June 2009.
- 39. Opačak, N.; Schwarz, B. Theory of Frequency-Modulated Combs in Lasers with Spatial Hole Burning, Dispersion, and Kerr Nonlinearity. *Phys. Rev. Lett.* **2019**, 123, 243902. [CrossRef]
- 40. Qi, X.; Kundu, I.; Dean, P.; Agnew, G.; Taimre, T.; Valavanis, A.; Grier, A.T.; Linfield, E.H.; Davies, A.G.; Indjin, D.; et al. Mode Selection and Tuning Mechanisms in Coupled-Cavity Terahertz Quantum Cascade Lasers. *IEEE J. Sel. Top. Quantum Electron.* 2017, 23, 12003125. [CrossRef]
- 41. Qi, X.; Agnew, G.; Taimre, T.; Han, S.; Lim, Y.L.; Bertling, K.; Demic, A.; Dean, P.; Indjin, D.; Rakić, A.D. Laser feedback interferometry in multi-mode terahertz quantum cascade lasers. *Opt. Express* **2020**, *28*, 14246–14262. [CrossRef]
- 42. Jirauschek, C.; Tzenov, P. Self-consistent simulations of quantum cascade laser structures for frequency comb generation. *Opt. Quantum Electron.* **2017**, 49, 414. [CrossRef]
- 43. Haus, H. Theory of mode locking with a slow saturable absorber. IEEE J. Quantum Electron. 1975, 11, 736–746. [CrossRef]
- 44. Perego, A.M.; Garbin, B.; Gustave, F.; Barland, S.; Prati, F.; De Valcárcel, G.J. Coherent master equation for laser modelocking. *Nat. Commun.* **2020**, *11*, 311–313. [CrossRef] [PubMed]
- 45. Menyuk, C.R.; Talukder, M.A. Self-Induced Transparency Modelocking of Quantum Cascade Lasers. *Phys. Rev. Lett.* **2009**, 102, 023903. [CrossRef]
- 46. Wang, C.Y.; Diehl, L.; Gordon, A.; Jirauschek, C.; Kärtner, F.X.; Belyanin, A.; Bour, D.; Corzine, S.; Höfler, G.; Troccoli, M.; et al. Coherent instabilities in a semiconductor laser with fast gain recovery. *Phys. Rev. A* **2007**, *75*, 031802. [CrossRef]
- 47. Villares, G.; Faist, J. Quantum cascade laser combs: Effects of modulation and dispersion. *Opt. Express* **2015**, 23, 1651–1669. [CrossRef]
- 48. Nabors, C.D.; Farinas, A.D.; Day, T.; Yang, S.T.; Gustafson, E.K.; Byer, R.L. Injection locking of a 13-W cw Nd:YAG ring laser. *Opt. Lett.* 1989, 14, 1189–1191. [CrossRef]
- 49. Ramos, R.T.; Gallion, P.; Erasme, D.; Seeds, A.J.; Bordonalli, A. Optical injection locking and phase-lock loop combined systems. *Opt. Lett.* **1994**, *19*, 4–6. [CrossRef]
- 50. Ahmad, F.R.; Rana, F. Fundamental and Subharmonic Hybrid Mode-Locking of a High-Power (220 mW) Monolithic Semiconductor Laser. *IEEE Photon-Technol. Lett.* **2008**, 20, 1308–1310. [CrossRef]
- 51. Viktorov, E.V.; Mandel, P.; Vladimirov, A.G.; Wolfrum, M.; Fiol, G.; Kuntz, M.; Bimberg, D. Hybrid Mode-Locking in a 40 GHz Monolithic Quantum Dot Laser. In Proceedings of the European Conference on Lasers and Electro-Optics, Munich, Germany, 14–19 June 2009. [CrossRef]
- 52. Ji, C.; Chubun, N.; Broeke, R.; Cao, J.; Du, Y.; Bjeletich, P.; Yoo, S. Electrical subharmonic hybrid mode locking of a colliding pulse mode-locked laser at 28 GHz. *IEEE Photon. Technol. Lett.* **2005**, *17*, 1381–1383. [CrossRef]
- 53. Adler, R. A study of locking phenomena in oscillators. Proc. IEEE 1973, 61, 1380–1385. [CrossRef]
- 54. Gellie, P.; Barbieri, S.; Lampin, J.-F.; Filloux, P.; Manquest, C.; Sirtori, C.; Sagnes, I.; Khanna, S.P.; Linfield, E.H.; Davies, A.G.; et al. Injection-locking of terahertz quantum cascade lasers up to 35 GHz using RF amplitude modulation. *Opt. Express* **2010**, *18*, 20799. [CrossRef]
- 55. Barbieri, S.; Maineult, W.; Dhillon, S.S.; Sirtori, C.; Alton, J.; Breuil, N.; Beere, H.E.; Ritchie, D. 13 GHz direct modulation of terahertz quantum cascade lasers. *Appl. Phys. Lett.* **2007**, *91*, 143510. [CrossRef]

Micromachines 2022, 13, 2063 18 of 18

56. St-Jean, M.R.; Amanti, M.I.; Bernard, A.; Calvar, A.; Bismuto, A.; Gini, E.; Beck, M.; Faist, J.; Liu, H.C.; Sirtori, C. Injection locking of mid-infrared quantum cascade laser at 14 GHz, by direct microwave modulation. *Laser Photonics Rev.* **2014**, *8*, 443–449. [CrossRef]

- 57. Wang, F.; Slivken, S.; Razeghi, M. Harmonic injection locking of high-power mid-infrared quantum cascade lasers. *Photon. Res.* **2021**, *9*, 1078. [CrossRef]
- 58. Paoli, T.; Ripper, J. Direct modulation of semiconductor lasers. Proc. IEEE 1970, 58, 1457–1465. [CrossRef]
- 59. Roy, R.; Schulz, P.A.; Walther, A. Acousto-optic modulator as an electronically selectable unidirectional device in a ring laser. *Opt. Lett.* **1987**, *12*, 672–674. [CrossRef]
- 60. Garside, B.K.; Lim, T.K. Laser mode locking using saturable absorbers. J. Appl. Phys. 1973, 44, 2335–2342. [CrossRef]
- 61. Brabec, T.; Spielmann, C.; Curley, P.F.; Krausz, F. Kerr lens mode locking. Opt. Lett. 1992, 17, 1292–1294. [CrossRef]
- 62. Wang, C.Y.; Kuznetsova, L.; Gkortsas, V.M.; Diehl, L.; Kärtner, F.X.; Belkin, M.; Belyanin, A.; Li, X.; Ham, D.; Schneider, H.; et al. Mode-locked pulses from mid-infrared Quantum Cascade Lasers. *Opt. Express* **2009**, *17*, 12929–12943. [CrossRef]
- 63. Oustinov, D.; Jukam, N.; Rungsawang, R.; Madéo, J.; Barbieri, S.; Filloux, P.; Sirtori, C.; Marcadet, X.; Tignon, J.; Dhillon, S. Phase seeding of a terahertz quantum cascade laser. *Nat. Commun.* **2010**, *1*, 69. [CrossRef]
- 64. Maysonnave, J.; Jukam, N.; Ibrahim, M.S.M.; Rungsawang, R.; Maussang, K.; Madéo, J.; Cavalié, P.; Dean, P.; Khanna, S.P.; Steenson, D.P.; et al. Measuring the sampling coherence of a terahertz quantum cascade laser. *Opt. Express* **2012**, 20, 16662. [CrossRef]
- 65. Hillbrand, J.; Andrews, A.M.; Detz, H.; Strasser, G.; Schwarz, B. Coherent injection locking of quantum cascade laser frequency combs. *Nat. Photon.* **2018**, *13*, 101–104. [CrossRef]
- 66. Bachmann, D.; Rösch, M.; Süess, M.J.; Beck, M.; Unterrainer, K.; Darmo, J.; Faist, J.; Scalari, G. Short pulse generation and mode control of broadband terahertz quantum cascade lasers. *Optica* **2016**, *3*, 1087. [CrossRef]
- 67. Lyakh, A.; Suttinger, M.; Go, R.; Figueiredo, P.; Todi, A. 5.6 μm quantum cascade lasers based on a two-material active region composition with a room temperature wall-plug efficiency exceeding 28%. *Appl. Phys. Lett.* **2016**, *109*, 121109. [CrossRef]